UC Berkeley
UC Berkeley Previously Published Works

Title
Thermodynamic, Kinetic, and Transport Contributions to Hydrogen Evolution Activity and Electrolyte-Stability Windows for Water-in-Salt Electrolytes

Permalink
https://escholarship.org/uc/item/4p3409pp

Journal
Journal of the American Chemical Society, 146(5)

ISSN
0002-7863

Authors
Zhao, Yang
Hu, Xudong
Stucky, Galen D
et al.

Publication Date
2024-02-07

DOI
10.1021/jacs.3c12980

Peer reviewed

eScholarship.org Powered by the California Digital Library
University of California

Thermodynamic, kinetic, and transport contributions to hydrogen evolution activity and electrolyte-stability windows for water-in-salt electrolytes

Yang Zhao[1], Xudong Hu[1], Galen D. Stucky[2], Shannon W. Boettcher[1]*

[1]*The Department of Chemistry and Biochemistry and the Oregon Center for Electrochemistry, University of Oregon, Eugene.*

[2]*Department of Chemistry and Biochemistry, University of California, Santa Barbara.*

ABSTRACT:

Concentrated water-in-salt electrolytes (WiSEs) are used in aqueous batteries and to control electrochemical reactions of water in fuel electroproduction. The hydrogen evolution reaction at is a parasitic reaction at the negative electrode that limits cell voltage and leads to self-discharge in batteries and affects selectivity in for electrosynthesis. Mitigating and modulating these processes is hampered by a limited fundamental understanding of HER kinetics in WiSEs. Here, we quantitatively assess how thermodynamics, kinetics, and interface layers control the apparent HER activities in 20 m LiTFSI. When the LiTFSI concentration is increased from 1 m to 20 m, an increase in proton activity causes a positive shift in the HER equilibrium potential of 71 mV. The exchange current density, i_0, derived from the HER branch for 20 m LiTFSI in 98% purity (0.56 ± 0.05 μA/cm$^2_{Pt}$), however, is 8 times lower than for 20 m LiTFSI in 99.95% (4.7 ± 0.2 μA/cm$^2_{Pt}$) and 32 times lower than for 1 m LiTFSI in 98% purity (18 ± 1 μA/cm$^2_{Pt}$) demonstrating that the WiSE's impurities and concentration are both central in significantly suppressing HER kinetics. The ability and applicability of the reported methods are confirmed by examining additional WiSEs formulations made of acetates and nitrates.

INTRODUCTION

Aqueous batteries have long been envisioned as a safe (non-flammable), green, and cost-effective energy-storage technology with the possibility for high power and energy density,[1,2] but historically have been limited by the water electrochemical stability window of ~1.23 V based on thermodynamics.[3] For some electrodes, the slow hydrogen and oxygen evolution kinetics allow working voltages >2 V, such as in the Pb-acid battery. Recently, "water-in-salt" electrolytes (WiSEs) have been prepared by dissolving large quantities of salt in small quantities of water.[4–10] With 21 mol kg^{-1} (21 m) aq. lithium bis(trifluoromethane) sulfonamide (LiTFSI)[4] the salt/water molar ratio (Li^+:H_2O) is 1:2.6. This electrolyte has a reported electrochemical stability window of ~ 3 V, resulting in a significant increase in aqueous battery energy density. Diverse electrolyte salts have now been used in WiSE systems[11–19] including nitrates,[5] acetates,[6] water-in-bisalt electrolytes (LiTFSI + LiOTf),[7] hydrate-melt electrolytes (LiTFSI + LiBETI)[7], and molecular crowding electrolytes (2 m LiTFSI in 94% PEG).[20]

Despite the tremendous effort in developing WiSEs that aim to offer high-voltage/high-energy batteries, the understanding of stability/instability[21] in WiSEs is constrained by the limited research on the individual effects of thermodynamic and kinetic factors from HER and OER.[22] It has been largely accepted, but without much direct proof, that a scarcity of free water molecules with reduced thermodynamic activity widens the overall voltage window, and the creation of protective solid-electrolyte interphase (SEI) layer at the negative electrode may further modulate kinetics.[4,23] Beyond battery applications, WiSEs are being used as advanced electrolytes for electrosynthesis, for example in CO_2 electroreduction where controlling the apparent 'activity' of water affects the selectivity and product distributions.[24–26]

For applications, understanding the HER, and more broadly interfacial electrode kinetics, in WiSEs is essential. Compared to the oxygen evolution reaction (OER), the HER has fast kinetics, thus is difficult to prevent, and is typically the cause of poor coulombic efficiency (CE) in aqueous batteries.[23,27,28] Zheng and Pan et al.[5] used a titration calorimetry experiment to analyze the thermodynamic extension of the electrochemical window of 22.2 m $LiNO_3$ and found little change to the underlying water-splitting thermodynamics, concluding that kinetic effects must dominate. Here we find that $LiNO_3$ is not a good WiSE for studying kinetics because of parasitic reactions

(discussed below). Several studies targeted understanding reactions on negative electrodes in WiSEs.[23,29,30] Wang and Suo et al. argue that the reduction of dissolved gas and $TFSI^-$ creates LiF, Li_2O, and Li_2CO_3 as protective barriers to inhibit H_2 evolution.[23] Grimaud and Dubouis et al. propose that the initial electrochemical reduction of water plays a role in catalyzing the formation of the SEI composed of LiF and CF_x.[29] Fontaine and Bouchal et al. assigned two distinct reduction potentials for the chemical environments of free and bound water.[30] They used online electrochemical mass spectrometry to show that water reduction is the only contributor to the reductive current, consistent with the findings of Dubouis et al,[30] and they suggested that tuning local salt precipitation/dissolution enables improved reductive stability. However, a key knowledge gap is how the kinetics for HER fundamentally depend on the nature of the electrolyte and double-layer environment, compared to possible modification of the solid-electrolyte interface. Further, due to the complex environment of water in WISEs,[24] even cleanly measuring the activity of protons, water, and separating thermodynamic from kinetic and interface-modification effects is a significant challenge.

Here we use a Pt rotating-disk electrode to study HER/HOR kinetics in WISE electrolytes under controlled mass-transport conditions. Pt is a fast (reversible kinetics) catalyst for HER/HOR in aqueous acid and thus measured changes to the Pt HER/HOR activity in the WISE should provide key information on operative mechanisms. We use measurements of water and proton activity to deconvolute thermodynamic and kinetic changes to the apparent potential-dependent HER/HOR current.

We find that the equilibrium/reversible-hydrogen potential shifted substantially for the different electrolytes studied apparently due to changes in proton activity. For example, a positive shift of hundreds of mV was observed going from acidic concentrated $LiNO_3$ to more-alkaline concentrated acetates. The decreased water activity, measured directly, has only a small effect (tens of mV) on the water-splitting thermodynamics. We also directly measure HER/HOR rates on a Pt rotating-disk electrode (RDE) and Pt-ring/Pt-disk electrode (RRDE), and quantitively determined the kinetic parameters (charge-transfer coefficient α, and exchange current density i_0) of various WiSEs, including LiTFSI and acetates. We find that WiSEs exhibit slow kinetics (lower than in 0.1 M NaOH). The level of HER/HOR kinetic inhibition appears governed by electrolyte concentration, as well as impurities in the electrolyte. Remarkably, commonly employed 98%

LiTFSI has slow HER/HOR kinetics but ultra-pure 99.95% has 8 times faster HER kinetics. We present here a comprehensive analysis for examining both thermodynamics and kinetics that can be used in a variety of settings involving aqueous concentrated electrolytes thus providing guidance for assessing WiSEs for practical use.

EXPERIMENTAL SECTION

Chemicals. All reagents were obtained commercially and used as received without any further purification. Lithium bis(trifluoromethanesulfonyl)imide (LiTFSI) (>98.0%) was obtained from Tokyo Chemical Industry. LiTFSI (99.95%), Lithium acetate ($LiOOCCH_3$, 99.95%), Potassium acetate (CH_3COOK, 99.98%), Lithium nitrate ($LiNO_3$, 99.99%), and Perchloric acid ($HClO_4$, 70%, 99.999% trace metals basis) were obtained from Sigma-Aldrich.

Measurement of water activity. Water activity was evaluated by sampling from the headspace of vials containing different concentrations of LiTFSI. This was accomplished by precisely measuring the humidity (RH) in the headspace of sealed vials using a Traceable® Thermohygrometer with calibration. The thermohygrometer sensor was snugly put into the vial through the custom cap and adjusted to headspace once the electrolytes were supplied. The vial was then sealed with a cap and Parafilm® double seal (**Figure S3**). The setup was left at room temperature for > 8 h to achieve vapor-liquid equilibrium before measuring humidity. A pure-water reference was prepared in addition to the electrolyte samples, offering a benchmark for unity water activity. According to the following equation, the water activity values for several LiTFSI electrolytes were determined:

$$a_{H_2O} = \frac{RH_{sample}}{RH_{Pure\ water}} \quad [1]$$

Preparation of platinized Pt. The platinized Pt electrode was prepared by electrochemically depositing Pt onto a commercial Pt wire (CHI, 0.5 mm diam, 32 mm length). Before platinization, the Pt wire was first cleaned in fresh aqua regia for 3 min, then it was cleaned electrochemically in Ar sat. 0.1 M $HClO_4$. The electrode was platinized in deposition bath of 0.072 M (3.5%) chloroplatinic acid[31] (saturated with Ar in advance) at a constant potential of 0.17 V vs. NHE for 15 min. Good stirring is found to be important for the deposition, and no gas should be evolved at the Pt cathode.

Electrochemical measurements. This work employed the mercury/mercurous-sulfate reference electrode for all electrochemical measurements. The HOR/HER activity measurements were performed using a rotating ring-disk electrode (RRDE, E6R1, disk outer diameter = 5.0 mm; ring outer diameter = 7.50 mm; ring inner diameter = 6.50 mm, Pine Research). Prior to the assembly of the electrode, the disk was hand-polished with 0.1 μm alumina suspension and ultrasonically cleaned in ultrapure water. Following the disk insertion, the assembled RRDE was hand-polished with 0.1 μm alumina suspension and ultrasonically cleaned again then subjected to an electrochemical cleaning procedure by immersing it in Ar saturated 0.1 M $HClO_4$ and recording cyclic voltammograms (CVs) between 0.05 V and 1.2 V vs. NHE at 200 mV/s, in 100-cycle intervals. The active surface area of Pt was determined from by integration of the Pt-H desorbtion wave, yielding 0.41 cm^2 for the Pt disk. The current densities stated in the paper were all normalized with actual surface area of Pt. The geometric area is 0.20 cm^2, which would yield geometric current densities about twice the microscopic current densities reported. The ohmic drop between the working and the reference electrode was quantified by electrochemical impedance spectroscopy (EIS), applying a 5 mV voltage perturbation (1 MHz to 10 Hz) at the open-circuit potential, to find the high-frequency series resistance. The *iR*-corrected potential was calculated from:

$$E_{iR\text{-corr.}} = E - iR \quad [2]$$

The NHE used throughout the paper was obtained from mercury-mercurous sulfate reference electrode measurement, taking the difference between the two as 0.615 V. We note this is an estimation due to the liquid junction potentials, but enables different electrolytes to be compared similarly in some cases. Specifically, for 20 m LiTFSI (98% purity): NHE = +0.37 V vs RHE; in 20 m LiTFSI (99.95% purity) NHE = +0.42 V vs RHE; in 16 m potassium acetate + 4 m lithium acetate NHE = +0.64 V vs RHE.

RESULTS AND DISCUSSION

Underlying thermodynamic, kinetic, and transport concepts governing WISEs. We first quantify how thermodynamic and kinetic factors affect both HER and the microscopically reverse hydrogen-oxidation reaction (HOR) activity in WiSEs.[32] Data relating to the electrochemical

window of highly concentrated electrolytes has been frequently discussed in terms of onset potentials (the potential required to achieve a specific electrochemical current density). Onset potentials are governed by thermodynamics, kinetics, and transport phenomena. Few reports discuss changes to the thermodynamic reversible/equilibrium potential of H_2O/H_2 in WiSEs.[33] The unusual properties of WiSEs, including lower water content and high viscosity, make the problem difficult and thus contribute substantially to the uncertainty.

We first consider the thermodynamics governing the stability window. The reversible potentials for HER and OER can be written either with protons or hydroxides.

$$2H_2O + 2e^- \rightleftarrows H_2 + 2OH^- \quad \text{or} \quad 2H^+ + 2e^- \rightleftarrows H_2 \qquad [3]$$

$$4OH^- \rightleftarrows O_2 + 2H_2O + 4e^- \quad \text{or} \quad 2H_2O \rightleftarrows O_2 + 4H^+ + 4e^- \qquad [4]$$

Because the proton and hydroxide activities are linked by the water dissociation reaction, $H_2O \leftrightarrow H^+ + OH^-$, the thermodynamic stability window for WISE electrolytes does not depend on which equilibria are considered, but only on the activities of water species in the overall chemical reaction, $H_2O \rightleftarrows H_2 + 1/2O_2$. The thermodynamic voltage window, assuming unit activity of O_2 and H_2 and room temperature, is thus:

$$E_{\mathrm{OER}} - E_{\mathrm{HER}} = E^{\circ}_{\mathrm{H_2O/O_2}} - E^{\circ}_{\mathrm{H_2/H_2O}} - \frac{RT}{2F}\ln\left(a_{H_2O}\right) = 1.23\ \mathrm{V} - \frac{RT}{2F}\ln\left(a_{H_2O}\right) \qquad [5]$$

R is the gas constant, 8.314 J/(mol·K), T is the temperature in Kelvin (298.15 K was used for calculations below), and F is the Faraday constant (96,485 C/mol). A decrease in a_{H_2O} (**Figure 1a** and discussed below) will result in a wider, more thermodynamically stable potential window.

Kinetic and transport effects, in addition to thermodynamics, also modulate the apparent voltage stability window of an electrolyte. Typically, the HER has orders of magnitude faster kinetics than the OER in aqueous electrolytes and is the focus of our work here. The HER kinetics might be slowed in WISE electrolytes due to changes in the chemical nature of water (i.e. fully coordinated by abundant cations),[29] the nature of the double layer (for example, crowded with cations that restrict water access to the surface where electron/proton transfer occurs through an inner-sphere process),[34] or the formation of a blocking solid-electrolyte-interface (SEI) layer.[4,29] All these effects are important to consider.

Transport effects have generally not been thoroughly discussed in the WISE literature. While the overall thermodynamics represented by **Eqn. [5]** do not depend on the particular pH, the lack of high proton or hydroxide concentrations in WISE electrolytes means that large pH gradients can develop when any of the reactions in **Eqns. [3]** or **[4]** are driven. One challenge is accurate measurements of the $pH = -\log(a_{H^+})$ in WISE electrolytes due to significant junction potentials when using typical laboratory pH probes;[33] we address this by using pH paper and direct measurements of the reversible hydrogen potential using high-surface-area Pt sensing electrodes (**Figure 1b**). Because the pH are all near neutral, the defining electrode reactions rapidly consume any OH^- or H^+ initially present near the electrode surface, leading to a pH gradient in the electrolyte. This induces a concentration (Nernst) overpotential that practically increases the voltage window. For example, consider the situation as is present in the WISE where water is a reactant at both anode and cathode after concentration polarization. The two reactions become:

$$2H_2O + 2e^- \rightleftarrows H_2 + 2OH^- \text{ and } 2H_2O \rightleftarrows O_2 + 4H^+ + 4e^- \quad [6]$$

These reactions generate protons at the anode and hydroxide at the cathode that work to increase the voltage, via a Nernst overpotential, needed to pass current. Small currents are likely sufficient to cause pH changes of several units at the electrode surfaces given the WISE electrolytes lack buffering capacity.

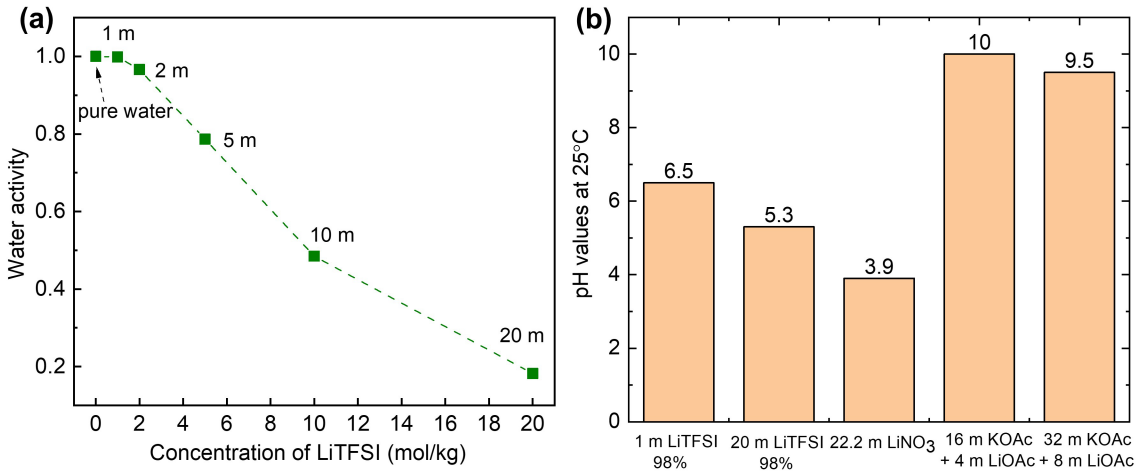


Figure 1. Water activity and the pH of WiSEs. (a) Water activity was measured at 25°C with a calibrated hygrometer for various concentrations of LiTFSI (98% in purity). (b) pH values were measured at 25°C with chemical indicated pH strips for various WiSEs.

Experimental measurements of water and proton activity in WISEs. We measured the humidity in the headspace of vials containing electrolytes with different water content in vapor-liquid equilibrium to obtain a_{H_2O} (**Figure S1**),[35] which decrease with the increasing LiTFSI concentration and reach a minimum of 0.18 in 20 m LiTFSI (**Figure 1a**). For 20 m LiTFSI, the reduced a_{H_2O} widens the potential window by 22 mV according to **Eqns. [5]**, which is a negligible increase and similar to the 15.5 mV increase Zheng et al.[5] reported from titration calorimetry for both concentrated $LiNO_3$ and LiTFSI. In addition, a series of LiTFSI electrolytes (of typically 98% purity) at 1 m, 2 m, 5 m, 10 m, and 20 m were prepared, and the pH was measured with glass-electrode pH meter, ISFET pH meter, and pH strips (**Figure S2**). Because electrolytes are not buffered, drifting readings were seen with both the glass-electrode pH meter and the ISFET pH meter. Although pH strips are typically inferior to pH meters, we found them superior for estimating proton activity in WiSEs due to the large junction potentials[33] across the pH electrodes when contacting concentrated electrolytes causing systematic errors that are difficult to correct for. Various brands of pH strips were screened, non-bleeding MQuant® was selected due to effective infiltration, fast response, and good color discrimination. Tests were performed in Ar-sparged sealed vials to exclude the influence of CO_2 in the air. The acidity of electrolytes directly correlated with concentration (**Figure 1b**). Compared to 1 m LiTFSI, an increase by 1.2 orders of magnitude of a_{H^+} appeared in 20 m LiTFSI, which yields a positive shift of E_{eq} for HER/HOR and OER/ORR of 71 mV, making water thermodynamically easier to reduce to H_2 on an absolute potential scale. The pH of multiple WiSEs including 22.2 m $LiNO_3$, 16 m KOAc + 4 m LiOAc, and 32 m KOAc + 8 m LiOAc were tested and these representative electrolytes exhibited large variations from acidic to alkaline. The pH changed from ~10.0 to 9.5 with increased concentration from 16 m KOAc + 4 m LiOAc to 32 m KOAc + 8 m LiOAc.

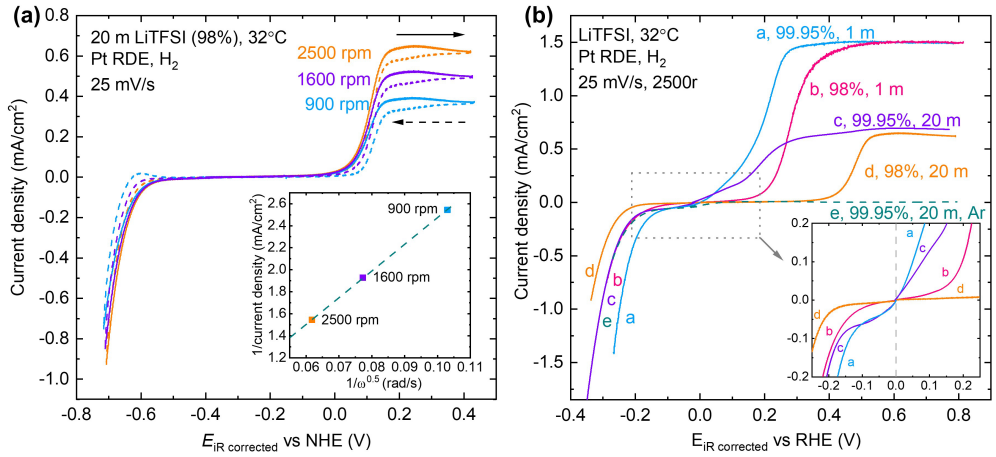


Figure 2. (a) CV scans of H_2 reduction and oxidation on Pt RDE at different rotation rates in H_2 sat. 20 m LiTFSI, recorded at 25 mV/s. The arrow indicates the scan direction. Inset shows the Koutecky-Levich analysis for the HOR currents at 0.25 V (vs. NHE). (b) H_2 reduction and oxidation currents on Pt RDE at 2500 rpm in various H_2 sat. LiTFSI electrolytes. Inset shows a zoomed plot.

Together, these results show that increasing the electrolyte concentration does not significantly increase the thermodynamic potential window. The shift caused by a pH change (in the absence of current) is also small, although will be considered in the context of kinetics below. WiSEs with mildly alkaline concentrated acetates have a more-negative E_{eq} for HER/HOR, helping to prevent the HER as a side reaction, while mildly acidic concentrated $LiNO_3$ in principle allows HER to occur at more positive potentials. However, as mentioned above, because neither is buffered and both pHs are near neutral, small amounts of electrolysis current will deplete the equilibrium proton or hydroxide content in the vicinity of the electrodes leading to pH gradients and likely little difference in apparent window based on the measured pH alone.

Experimental measurements of thermodynamic potentials and HOR/HER kinetics. Rotating-disk electrodes (RDEs) provide steady-state laminar flow conditions adjacent to the electrode surface and thus are commonly used to quantify electrode reaction kinetics.[32,36,37] We performed HOR/HER in H_2-saturated 20 m LiTFSI using a Pt RDE at different rotating rates (900 rpm, 1600 rpm, and 2500 rpm). H_2 oxidation reaches diffusion limitation at ~ 0.2 V to 0.4 V vs. NHE at 32°C (**Figure 2a**). This temperature was chosen to avoid salt precipitation, which was observed during H_2 purging at room temperature. Koutecky-Levich analysis at 0.25 V vs. NHE (**Figure 2a, inset**)

shows that the diffusion-limited currents have the expected rotation-speed dependence in the presence of H_2, confirming well-defined mass transport conditions.

We must first know E_{eq} of HER/HOR in WiSEs to have a fundamental understanding of the kinetics. Although we approximated that E_{eq} varies within a scale of 100 mV, as described above, it depends on the activity of all the species, including protons, water, and hydroxides, and is difficult to precisely calculate given uncertainties in single-ion activity measurements in concentrated electrolytes. We measured E_{eq} directly by open-circuit potential (OCP) measurements at Pt electrodes in equilibrium with dissolved H_2 at 1 atm. While reference-electrode junction potentials make the absolute value of the measured E_{eq} uncertain,[35] the equilibrium potential is a well-defined quantity from which the current response to applied overpotential can be measured precisely and equilibrium-exchange currents calculated.

We first examined the reversible hydrogen-electrode potential, RHE, in 20 m LiTFSI (98%). To make accurate and reproducible OCP measurements, platinized Pt electrodes with ~500 times more active surface area than the Pt RDE were used (**Figure S3**). The overpotentials for subsequent HOR/HER kinetic measurements under well-defined mass transfer conditions (Pt RDE, 2500 rpm, H_2 sat.) were found by referencing to this experimentally measured RHE.

CV scans of 20 m LiTFSI (99.95%), 1 m LiTFSI (99.95%), and 1 m LiTFSI (98%) were collected (**Figure S4**). When compared to 1 m LiTFSI, 20 m LiTFSI has much slower kinetics. Further, we discovered that the HER/HOR kinetics in LiTFSI depend strongly on the electrolyte purity level (**Figure 2b**), with 99.95% electrolytes having much faster kinetics than 98% electrolytes. This has not been previously reported but is central to fundamentally understanding WISEs as well as applying them in practical batteries or for electrosynthetic reactions. 20 m LiTFSI and 1 m LiTFSI with 98% purity exhibited a wide plateau with a current density close to zero at the potential window of ca. -0.2 V to 0.3 V vs. RHE and ca. -0.1 V to 0.1 V vs. RHE, respectively, consistent with the ability to suppress electrolyte water decomposition and practically leading to the wider electrolyte stability window often reported.

In contrast in high-purity 20 m and 1 m LiTFSI (99.95%), a low-current-density region between 0 V to -0.1 V and 0 V to -0.15 V vs. RHE appeared, respectively. The onset potential of HOR in 20 m LiTFSI (99.95%) was ~0.3 V negative (i.e. more favorable) of that in 20 m LiTFSI

(98%), and the same trend was observed in 1 m LiTFSI. Voltammetry in 20 m LiTFSI (99.95%, sparged with Ar) had negligible current between 0 V to 0.4 V vs. RHE, confirming that the current over the same region with H_2 is HOR. Even 1 m LiTFSI at 98% purity has slower kinetics than 20 m LiTFSI at 99.95%. Remarkably, impurities have a greater inhibitory effect on HER/HOR than does the concentrated electrolyte. Previous WiSE mechanistic studies[4,5,23,30] used only lower purity LiTFSI from 98% to 99%, and the new measurements here provide possible alternative interpretations. Clearly, interfaces and interface effects are particularly sensitive to impurities,[38–40] and this is critical to understand in the WISE system.

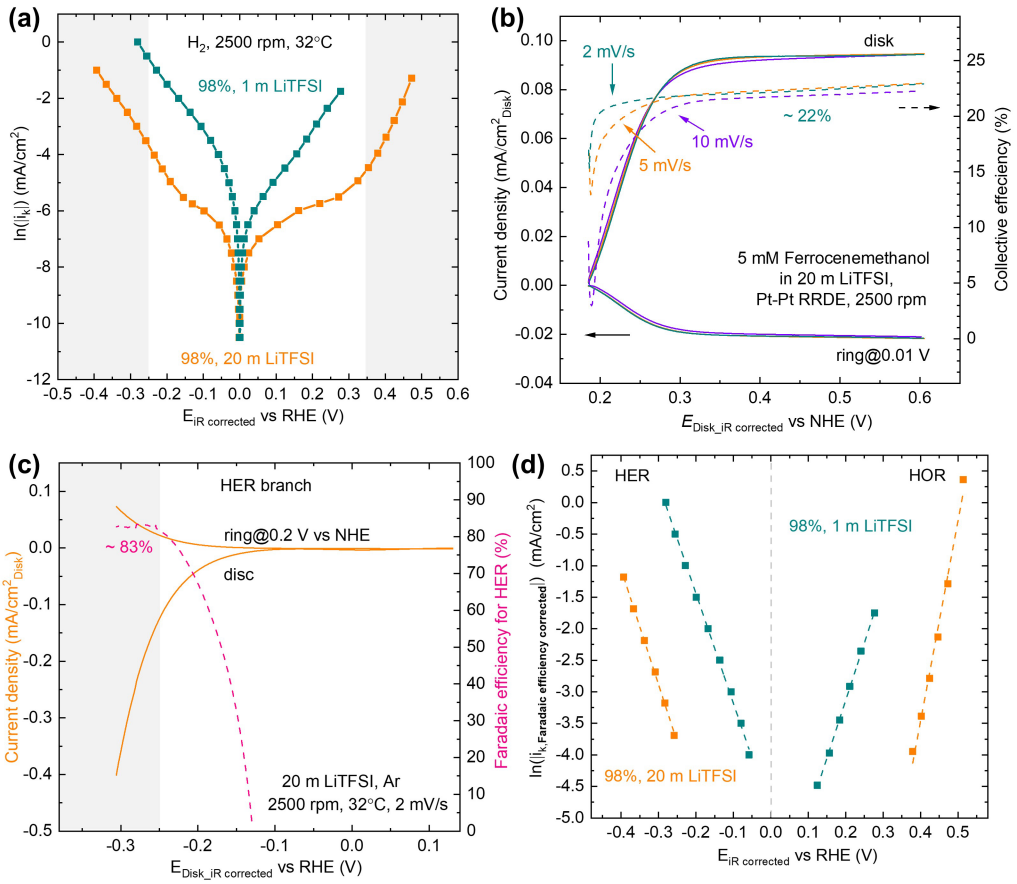


Figure 3. (a) Tafel plots of HOR/HER in 1 m LiTFSI and 20 m LiTFSI in 98% purity at a rotation speed of 2500 rpm after correction for mass transport overpotential due to H_2 diffusion. (b) Empirical measurement of the collection efficiency of Pt-Pt RRDE in 20 m LiTFSI containing 5 mM ferrocenemethanol at 10 mV/s, 5 mV/s, and 2 mV/s. (c) H_2 collection experiments on Pt-Pt RRDE in 20 m LiTFSI, solid lines represent disk and ring current, and the dashed line represents faradaic efficiency of HER derived accordingly. (d) Tafel

plots of HOR/HER in 1 m LiTFSI and 20 m LiTFSI in 98% purity at a rotation speed of 2500 rpm with further correction of Faradic efficiency for the derivation of kinetic parameters.

Table 1. Summary of kinetic parameters.

electrolyte	charge transfer coefficient, α	exchange current density, i_0 (A/cm^2)
20 m LiTFSI (HER, 98%)	0.48 ± 0.01	(5.6 ± 0.5) × 10^{-7}
1 m LiTFSI (HER, 98%)	0.46 ± 0.01	(1.8 ± 0.1) × 10^{-5}
20 m LiTFSI (HOR, 98%)	0.83 ± 0.04	(2.3 ± 1.7) × 10^{-10}
1 m LiTFSI (HOR, 98%)	0.48 ± 0.01	(2.8 ± 0.2) × 10^{-6}

For quantitative kinetic analysis, we compared 1 m LiTFSI and 20 m LiTFSI of 98% purity. **Figure 3a** shows steady-state Tafel plots collected by chronoamperometry at a fast rotation rate of 2500 rpm (**Figure S5**). The measured overpotentials include both the kinetic and mass-transport overpotentials. The kinetic current (i_k) can be thought of as the (higher) current that would be obtained if the system were under pure kinetic control with no mass transfer effects:

$$\frac{1}{i} = \frac{1}{i_k} + \frac{1}{i_d} \quad [7]$$

The term i_d is the diffusion-limited current, and is proportional to the limiting current i_l at a given potential by:

$$i_d = i_l \left(1 - \exp\left(-\frac{2F\eta_d}{RT}\right)\right) \quad [8]$$

where η_d is the diffusion/concentration/mass-transport overpotential.

The HER/HOR activity is characterized by the exchange current density (i_0), which is obtained by fitting the kinetic current (i_k) with the Butler-Volmer equation:

$$i_k = i_o \left(\exp\left(\frac{\alpha_a F\eta}{RT}\right) - \exp\left(-\frac{\alpha_c F\eta}{RT}\right)\right) \quad [9]$$

where α_a and α_c are the transfer coefficients for HOR and HER, respectively, and η is the overpotential. **Figure 3a** shows that the kinetic current for both HER and HOR in 20 m LiTFSI is significantly less than that in 1 m LiTFSI.

Previously it was reported that SEI layers develop under negative polarization due to reduction of $TFSI^-$ in 20 m LiTFSI,[4] which often occurs at potentials near that of HER. We thus

used RRDE experiments to quantitatively measure the fraction of current going to HER versus other faradaic reactions that might be associated with electrolyte or impurity reactions forming SEI layers or other passivating surface chemistries. First, we used $FcCH_2OH$ (ferrocenemethanol) / $FcCH_2OH^+$ (**Figure 3b**), an electrochemically reversible couple,[41] to quantify the collection efficiency of Pt-Pt RRDE in the WISEs. $FcCH_2OH$ and $FcCH_2OH^+$ are both soluble in low- and high-concentration aq. electrolytes in which commonly used species like $K_3Fe(CN)_6$ or ferrocene are not. The measured ratio of the ring current (the $FcCH_2OH^+$ generated from the oxidation of $FcCH_2OH$ at the disk, reduced back to $FcCH_2OH$) to the disk current (oxidation of $FcCH_2OH$ to $FcCH_2OH^+$) indicates an empirical collection efficiency was 23.5% in typical 1.0 M electrolytes (**Figure S6)** and ~22% in the more-viscous 20 m LiTFSI (**Figure 3b**). We also noticed that at a scan rate of 10 mV/s a time delay in achieving constant collection efficiency was found for potentials < 0.35 V vs. NHE at the disk (**Figure 3b**). This result contrasts with dilute electrolyte (**Figure S6b**), likely due to higher viscosity and longer disk-ring transit time in concentrated electrolyte. The collection efficiency was constant when the scan rate was reduced to 2 mV/s; this was used in subsequent RRDE measurements on concentrated electrolytes with a collection efficiency of 22% to correct for Faradaic efficiency. In 20 m LiTFSI, the faradaic efficiency for H_2 increases with negative overpotential yielding only 83% at -0.3 V versus RHE (**Figure 3c**); parasitic reactions are occurring, perhaps leading to SEI layer formation (discussed more below). In 1 m LiTFSI, on the other hand, we found a ca. 100% faradaic efficiency for H_2 (**Figure S6d**).

The kinetic current i_k at the HER branch in the Tafel plot (**Figure 3d**), within the potential region where collection efficiency is constant, was corrected by the Faradaic efficiency to determine kinetic parameters (**Table 1**). The HER and HOR currents for 1 m LiTFSI are reasonably symmetric (**Figure 3d**), with the sum of transfer coefficients close to 1. On the other hand, the kinetics for 20 m LiTFSI (typical purity of 98%) is much slower with the apparent i_0 from the HER branch reduced by a factor of ~32. For the HOR branch, the apparent i_0 was 10^4 times lower for 20 m LiTFSI than for 1 m. The difference between i_0 for HER and HOR branches may indicate that electrolyte impurities block H_2 transfer to the electrode surface during HOR. However, when kept at a constant positive polarization current, neither electrolyte was able to reach a stable potential for accurate steady state Tafel analysis (**Figure S7**). Consequently, the analysis that followed was focused on HER branches (**Figure S8a, Figure S8b**).

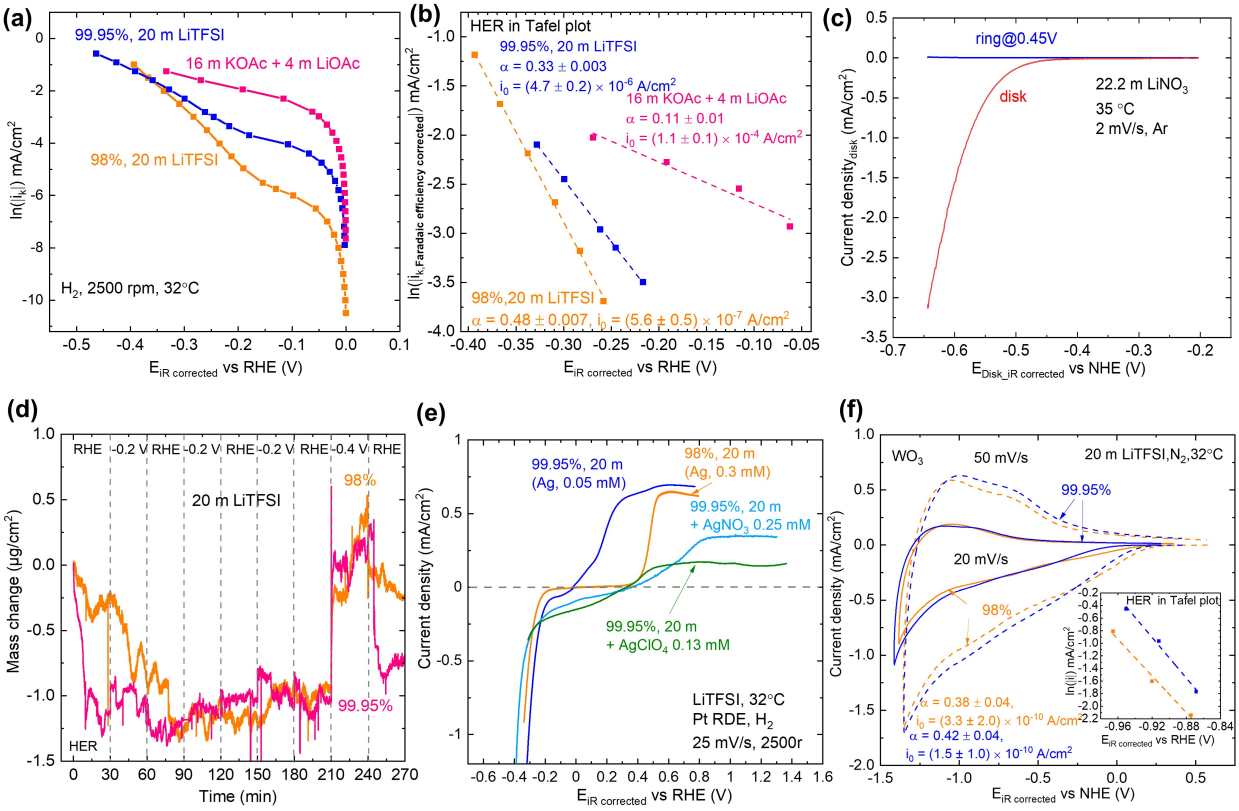


Figure 4. (a) Tafel plots of HOR/HER in 20 m LiTFSI (99.95%), 20 m LiTFSI (98%), and 16 m KOAc + 4 m LiOAc, respectively, at a rotation speed of 2500 rpm after correction for H_2 mass-transport overpotential. (b) Tafel plots of HER in above electrolytes with further faradaic efficiency correction and derived kinetic parameters including transfer coefficient, α, and exchange current density, i_0 accordingly. (c) H_2 collection experiments on Pt-Pt RRDE in Ar-sat. 22.2 m $LiNO_3$ at 35 °C. (d) Mass change recorded on a Pt electrochemical quartz microbalance electrode in 20 m LiTFSI (98%) and 20 m LiTFSI (99.95%) when switching potential between -0.2 V / -0.4 V vs. RHE and RHE, each potential was held for as long as 30 min. (e) CV scans of H_2 reduction and oxidation on Pt RDE at different rotation rate of 2500 rpm in H_2 sat. 20 m LiTFSI (99.95%) which was found to have 0.05 mM Ag impurities, 20 m LiTFSI (98%) which was found to have 0.3 mM Ag impurities, 20 m LiTFSI (99.95%) with 0.25 mM $AgNO_3$ intentionally added, 20 m LiTFSI (99.95%) with 0.13mM $AgClO_4$ intentionally added, all recorded at 25 mV/s. (f) CV scans in 20 m 99.95% LiTFSI with WO_3 as the working electrode with the inset showing the Tafel analysis from steady-state current for HER on WO_3.

Electrolytes of 20 m LiTFSI (high purity, 99.95%) and 16 m KOAc + 4 m LiOAc were also evaluated using the same procedures (due to precipitation under H_2 purging at 32 °C, 32 m KOAc + 8 m LiOAc was not examined). The mixed-acetate electrolyte showed an i_0 of (1.1 ± 0.1) × 10^{-4} A/cm^2, larger than the two 20 m LiTFSI electrolytes (**Figure 4a**). The high purity 20 m LiTFSI had an i_0 that is ~8 times larger than the normal purity salt. All the WiSEs that were investigated here have slower kinetics for HER than alkaline 0.1 M NaOH. Typical 98% purity 20 m LiTFSI (slightly acidic, pH = 5.3) exhibits the slowest kinetics with an i_0 1000 times lower than in 0.1 NaOH (i_o ~7 × 10^{-4} A/cm^2 at 32°C, which is much slower than in acid).[42,43] We also studied 22.2 m $LiNO_3$ at 35 °C (**Figure S8c**), which has been purported to have an aqueous stability window of ~2.5 V without creating a protective SEI.[5] However, our measurements show almost no HOR current at the ring, even though there is substantial current at the disk (**Figure 4c**). This is likely due to nitrate reduction, which is chemically unstable and is reduced via multiple mechanisms making this electrolyte likely unsuitable for batteries or reductive electrosynthesis.[44]

The loss of 17% of the negative current to parasitic electrolyte reactions, and the increased overpotential at positive polarization, in 20 m LiTFSI (98%) prompted us to study this system more closely. The loss of Faradaic efficiency was also observed in 20 m LiTFSI of 99.95% purity (**Figure S8a**) and 16 m KOAc + 4 m LiOAc (**Figure S8b**). Since fluorine, which was thought to be essential for the formation of SEI,[4,29,30] is absent in concentrated acetates, the loss in Faradaic efficiency apparently originates from other processes. Moreover, the Faradaic efficiency rapidly reaches high values in 20 m LiTFSI of 99.95% purity and in 16 m KOAc + 4 m LiOAc after passing negative of RHE (**Figure S8d**). However, in 20 m LiTFSI of 98% purity, passivation apparently occurs from 0 V to ~ -0.2 V vs RHE.

We also assessed the potential of zero free charge (PZFC) for the Pt in the various electrolytes, as the PZFC value (relative to RHE) is thought to affect HER/HOR kinetics.[45] It is known that the reduction of peroxydisulfate ($S_2O_8^{2-}$) is highly sensitive to the PZFC,[46] and that the onset of reduction current various with crystal facet as well as for different terrace and step-edge structures. We found onset for peroxydisulfate reduction on the polycrystalline Pt at ~ 0.8 V vs RHE in concentrated electrolytes of 20 m LiTFSI and 10 m LiTFSI, which suggests a PZFC in the double-layer region, and close to that reported elsewhere.[47] We also noted that in 10 m LiTFSI, at the same

concentration of peroxydisulfate, a larger peroxydisulfate reduction peak was found, indicating a $TFSI^-$ absorption is modulating the results.[48]

Microbalance measurements of passivation formation and stripping. We then used a Pt/Ti-coated electrochemical quartz-crystal microbalance (EQCM) to study mass changes associated with the cathodic and anodic currents. We assessed the effects of stirring and H_2 generation under negative polarization in 0.1 M $HClO_4$ and found that stirring caused a perturbation of only ~0.03 $\mu g/cm^2$ at open circuit (**Figure S9a**), and the generation and buildup of H_2 bubbles on the surface induced a perturbation of < 0.15 $\mu g/cm^2$ under negative polarization (**Figure S9b**) at up to -5 mA/cm^2.

Then the mass variation on Pt was monitored in concentrated electrolytes. No reproducible changes in mass were found for 20 m LiTFSI in purity of 98% and 99.95% at -0.2 V vs. RHE (**Figure 4d**). When -0.4 V vs RHE was applied, then removed, the mass returned closer to the initial mass at RHE for 20 m 99.95% LiTFSI. This reversible mass accumulation aligns well with the findings of prior study, which may be attributed to the adsorption of $Li(H_2O)^{n+}$ on the electrode surface.[29] However in 20 m 98% LiTFSI, additional irreversible mass accumulation was observed. If the measurements were taken over a longer period (**Figure S10a**), the mass increased by 2 to 3 $\mu g/cm^2$ after 3 h. The part of irreversible mass accumulation may be attributed to impurities present in the LiTFSI salt in purity of 98%.

X-ray photoelectron spectroscopy (XPS) measurements (**Figure S11**) were conducted on the Pt/Ti quartz crystal following its exposure to LiTFSI in 98%, which revealed a prominent signal from Ag on the surface. Consequently, we performed inductively coupled plasma-mass spectrometry (ICP-MS) measurements on both LiTFSI salts with purities of 98% and 99.95% (**Table S1**). At a concentration of 1.5 g/L of LiTFSI salt, the sample with a purity of 98% contained ~5 times more Ag (32.2 ± 0.1 ppb) compared to the sample with a purity of 99.95% (5.5 ± 0.1 ppb). In the 20 m concentrated electrolytes, 0.05 mM of Ag was thus in 99.95% LiTFSI and 0.3 mM in 98% LiTFSI.

To test if Ag is contributing to the modulation of electrode kinetics, we added extra 0.25 mM of Ag in the form of $AgNO_3$ to a 20 m 99.95% LiTFSI (which already contains 0.05 mM Ag). A substantial suppression in the HER kinetics and a significant passivation in the HOR region were

observed. This is consistent with the results obtained from the Tafel analysis discussed previously, which indicate that the kinetics of the hydrogen oxidation reaction (HOR) branch are substantially suppressed in a 20 m concentration of LiTFSI with 98% purity. It is also consistent with the very slow HOR and HER kinetics for Ag.[43,49,50] To assess the effect of concentration and anion, we also added 0.13 mM of Ag in the form of $AgClO_4$ to a 20 m 99.95% LiTFSI and found even more severe effects on electrode kinetics.

When a bias of 0.4 V vs. RHE or even 1.4 V vs. RHE was applied in 20 m LiTFSI (98%) for EQCM studies, no reproducible changes in mass were found, suggesting the Ag deposits are small in mass at HOR branch. We did notice the QCM resonance frequency drifted more substantially in WiSEs compared to typical electrolytes; this is likely due to the increased viscosity and thus substantially decreased quality factor of the QCM resonator (**Figure S9c**).[51,52] For 20 m LiTFSI the full-width-at-half-maximum in frequency of the crystal conductance increases by ~7 fold compared to in 0.1 M $HClO_4$ and by ~85 fold compared to in the air, indicating a resulting uncertainty in finding the resonance frequency in 20 m LiTFSI.

The cathodic mass deposition is consistent with the hypothesis that the loss of Faradaic efficiency of HER for negative current is partially due to reversible adsorption of $Li(H_2O)^{n+}$ and extra adsorption/deposition of Ag impurity for LiTFSI in 98% purity. It appears that the formation of SEI from decomposition in the concentrated electrolyte did not substantially occur over the potential region > -0.4 V vs RHE investigated here, despite large effects on kinetics. We note this range is somewhat more positive than reported SEI formation potential (< -0.8 V vs RHE) elsewhere.[29] The irreversible mass accumulation appeared to be more significant in 16 m KOAc + 4 m LiOAc (**Figure S10c**), however not overpotential/bias related when data was corrected with RHE drifting as a reference (**Figure S10d**). This may be attributed to the salt participation on the surface of electrode as previously reported in concentrated electrolyte,[30] which also explains the continues decrease in Faradaic efficiency of HER in 16 m KOAc + 4 m LiOAc from 0 V to -0.3 V vs RHE.

Effects of impurities on HER during oxide lithiation. While the above data indicate that the HER/HOR kinetics are substantially affected by impurities in WiSE electrolytes, for example Ag, it is useful to consider if they might also effect related processes on negative electrode materials.

As a model negative-electrode material, we use WO_3 thin films which we prepared via physical vapor deposition of 80 nm of WO_3 onto FTO.[53,54] WO_3 undergoes Li^+ insertion and de-insertion while charging and discharging:

$$WO_3 + xLi^+ + xe^- \rightarrow Li_xWO_3 \quad [10]$$

Voltammetry of WO_3 in 20 m LiTFSI (99.95% purity) showed reversible intercalation (**Figure 4f**). At more negative potentials, the occurrence of HER as a side reaction becomes apparent. A current-time transient was then captured by applying a constant potential to the electrode (**Figure S12**). As time progresses, the current reaches a small steady state, consistent with residual HER current. Taking the steady state (nominally HER) current as a function of electrode potential, we used Tafel analysis to find i_o of between 1 - 3 × 10^{-10} A/cm^2 for HER on WO_3 in both low and high purity LiTFSI, with the lower purity salt yielding roughly half the HER current at each potential.

It is known that Ag exhibits poor catalytic activity for both HOR and HER due to its high hydrogen adsorption energies of 0.3 – 0.4 eV (resulting in a greater energy requirement for the detachment of hydrogen, so desorption limits the overall rate) with exchange current densities of 10^{-7} to 10^{-8} A cm^{-2} in acidic and alkaline environments, in contrast to Pt (exchange current densities ranging from 10^{-1} to 10^{-3} A cm^{-2}).[43,50] Interestingly, WO_x and MoO_x, catalyze HER with an exchange current density that is about one magnitude greater than Ag,[49] consistent with the evident poising of HER kinetics on WO_3 we observe here. We note that this experiment was not completed with an RDE/RRDE, given the restrictions on easily accessible disk materials, and thus the quantification of Faradaic efficiency is not strictly accounted for. However, at steady state we expect the current to be dominated by HER over the potential region studied as the ion-insertion current decays to zero at a given applied voltage.

CONCLUSION

Careful measurements of HER activity in water-in-salt electrolytes show multiple effects central to understanding the expanded practical electrochemical window. Thermodynamically, increasing concentration from dilute to the solubility limit does not significantly increase the electrolyte stability window, while the equilibrium potential for HER

does move positively or negatively by tens to hundreds of mV due to the different pH of the electrolytes. The pH effect depends on the concentration and components of the electrolytes. Kinetically, the activity of HER is suppressed in WiSEs even without SEI formation, which in part is likely due to the formation of pH gradients and lack of buffering species. Concentration, electrolyte compositions, and salt impurities all further influence kinetics. When comparing 20 m LiTFSI at purities of 98% and 99.95%, the impurities reduce by 8 times i_0 for the HER on a Pt disk. In addition, i_0 for HER on Pt in 20 m LiTFSI in 98% is 32 times lower than in 1 m. SEI generation on negative electrodes in WiSEs has been the topic of numerous studies,[5,29,30] however without consideration of electrolyte impurities. These findings suggest that further performance engineering can take advantage of these effects, like in non-aqueous battery electrolytes, by using controlled additives in the electrolyte to build the SEI as opposed to relying on unknown impurities in the salt.[55] A key new impurity identified was Ag, although additional trace transition metal or other impurities, are likely.

It is also useful to discuss our findings in the context of previous conclusions in the literature. It is frequently stated that the onset potential/cathodic limit for HER in concentrated and diluted electrolytes are similar or the same.[5,29] Our results suggest that the "seemingly unchanged" onset potential for HER in many cases may be due to a combination of positive shifts from liquid junction potentials[33] and pH increase in WiSEs, along with a counteracting negative shift from the much slower kinetics. All these effects are likely to be modulated by the local environment, such as when different electrodes or various WiSEs are used. Given that kinetics typically increase exponentially with temperature, while thermodynamic parameters have a much weaker dependence, our findings are also consistent with observations that WiSE-based batteries have inferior temperature stability and that the rates of parasitic processes like HER increase at higher temperatures.[56]

The approach developed here, combining different measurements to understand how each of transport, kinetics, and thermodynamics together modulate rates of interface electrochemical processes in electrolytes, and thus the practically relevant electrolyte-stability window, is of broad utility in understanding fundamental aspects of, and design rules for, advanced aqueous electrolytes more broadly. Beyond battery applications, the reported understanding of WiSEs and related advanced electrolytes may be of substantial interest to

fields like electrochemical CO_2 and N_2 reduction, where the HER is also a parasitic reaction and precise interface microenvironment control is key to progress.[25,26,57–63]

ASSOCIATED CONTENT

Supporting Information

Summary of water activity measurement via hygrometer; pH values of LiTFSI electrolytes measured from various methods; voltammetric data of platinized Pt wire vs. Pt RDE; CV scans of HER and HOR at various rotation rates in LiTFSI electrolytes; chronopotentiometry on Pt RDE in 20 m LiTFSI (98%); summary of CV scans for ferrocenemethanol with Pt RDE and Pt-Pt RRDE; chronopotentiometry on Pt RDE in 20 m LiTFSI (99.95%) and 16 m KOAc + 4 m LiOAc; H_2 collection experiments on Pt-Pt RRDE in 20 m LiTFSI (99.95%), 16 m KOAc + 4 m LiOAc, and 22.2 m $LiNO_3$; mass change recorded on a Pt electrochemical quartz microbalance electrode in 0.1 M $HClO_4$; mass change recorded on a Pt electrochemical quartz microbalance electrode in 20 m LiTFSI (98%) and 16 m KOAc + 4 m LiOAc; XPS indicating the presence of Ag on Pt quartz crystal after EQCM measurements; *i-t* curves under various constant potential pulses in 20 m LiTFSI when WO_3 employed as working electrode; peroxodisulfate anion reduction CV on Pt disk in 20 m and 10 m LiTFSI; concentration of Ag in LiTFSI from the ICP-MS data.

AUTHOR INFORMATION

Corresponding Author

Shannon W. Boettcher – Department of Chemistry and Biochemistry, The Materials Science Institute, and the Oregon Center for Electrochemistry, University of Oregon, Eugene, OR 97403, United States; orcid.org/ 0000-0001-8971-9123; Email: swb@uoregon.edu

Authors

Yang Zhao – Department of Chemistry and Biochemistry, The Materials Science Institute, and the Oregon Center for Electrochemistry, University of Oregon, Eugene, OR 97403, United States; orcid.org/0000-0002-5252-6157

Xudong Hu – Department of Chemistry and Biochemistry, The Materials Science Institute, and the Oregon Center for Electrochemistry, University of Oregon, Eugene, OR 97403, United States; orcid.org/0000-0002-2141-5657

Galen D. Stucky – Department of Chemistry and Biochemistry, University of California Santa Barbara, Santa Barbara, California 93106, United States; orcid.org/ 0000-0002-0837-5961

ACKNOWLEDGMENTS

This work was supported by the U.S. Department of Energy, Office of Science, Office of Basic Energy Sciences, Fuels from Sunlight Hub under Award DE-SC0021266 (Y.Z. and S.W.B.). Y.Z., X.D.H., and G.D.S. acknowledge additional support from the Mitsubishi Chemical Center for Advanced Materials. Y.Z. acknowledges support and valuable discussions from Liam Twight, Kasinath Ojha, Caitlyn Cannan, Minkyoung Kwak, and Aaron Kaufman.

REFERENCES

(1) Kim, H.; Hong, J.; Park, K.-Y.; Kim, H.; Kim, S.-W.; Kang, K. Aqueous Rechargeable Li and Na Ion Batteries. *Chem. Rev.* **2014**, *114* (23), 11788–11827.

(2) Chao, D.; Zhou, W.; Xie, F.; Ye, C.; Li, H.; Jaroniec, M.; Qiao, S.-Z. Roadmap for Advanced Aqueous Batteries: From Design of Materials to Applications. *Sci. Adv.* **2020**, *6* (21), eaba4098.

(3) Chao, D.; Qiao, S.-Z. Toward High-Voltage Aqueous Batteries: Super- or Low-Concentrated Electrolyte? *Joule* **2020**, *4* (9), 1846–1851.

(4) Suo, L.; Borodin, O.; Gao, T.; Olguin, M.; Ho, J.; Fan, X.; Luo, C.; Wang, C.; Xu, K. "Water-in-Salt" Electrolyte Enables High-Voltage Aqueous Lithium-Ion Chemistries. *Science* **2015**, *350* (6263), 938–943.

(5) Zheng, J.; Tan, G.; Shan, P.; Liu, T.; Hu, J.; Feng, Y.; Yang, L.; Zhang, M.; Chen, Z.; Lin, Y.; Lu, J.; Neuefeind, J. C.; Ren, Y.; Amine, K.; Wang, L.-W.; Xu, K.; Pan, F. Understanding Thermodynamic and Kinetic Contributions in Expanding the Stability Window of Aqueous Electrolytes. *Chem* **2018**, *4* (12), 2872–2882.

(6) Lukatskaya, M. R.; Feldblyum, J. I.; Mackanic, D. G.; Lissel, F.; Michels, D. L.; Cui, Y.; Bao, Z. Concentrated Mixed Cation Acetate "Water-in-Salt" Solutions as Green and Low-Cost High Voltage Electrolytes for Aqueous Batteries. *Energy Environ. Sci.* **2018**, *11* (10), 2876–2883.

(7) Yamada, Y.; Usui, K.; Sodeyama, K.; Ko, S.; Tateyama, Y.; Yamada, A. Hydrate-Melt Electrolytes for High-Energy-Density Aqueous Batteries. *Nat. Energy* **2016**, *1* (10), 16129.

(8) Li, M.; Wang, C.; Chen, Z.; Xu, K.; Lu, J. New Concepts in Electrolytes. *Chem. Rev.* **2020**, *120* (14), 6783–6819.

(9) Borodin, O.; Self, J.; Persson, K. A.; Wang, C.; Xu, K. Uncharted Waters: Super-Concentrated Electrolytes. *Joule* **2020**, *4* (1), 69–100.

(10) Lannelongue, P.; Bouchal, R.; Mourad, E.; Bodin, C.; Olarte, M.; le Vot, S.; Favier, F.; Fontaine, O. "Water-in-Salt" for Supercapacitors: A Compromise between Voltage, Power Density, Energy Density and Stability. *J. Electrochem. Soc.* **2018**, *165* (3), A657–A663.

(11) Xu, J.; Ji, X.; Zhang, J.; Yang, C.; Wang, P.; Liu, S.; Ludwig, K.; Chen, F.; Kofinas, P.; Wang, C. Aqueous Electrolyte Design for Super-Stable 2.5 V $LiMn_2O_4$ || $Li_4Ti_5O_{12}$ Pouch Cells. *Nat. Energy* **2022**, *7* (2), 186–193.

(12) Dubouis, N.; Marchandier, T.; Rousse, G.; Marchini, F.; Fauth, F.; Avdeev, M.; Iadecola, A.; Porcheron, B.; Deschamps, M.; Tarascon, J.-M.; Grimaud, A. Extending Insertion Electrochemistry to Soluble Layered Halides with Superconcentrated Electrolytes. *Nat. Mater.* **2021**, *20* (11), 1545–1550.

(13) Chen, L.; Zhang, J.; Li, Q.; Vatamanu, J.; Ji, X.; Pollard, T. P.; Cui, C.; Hou, S.; Chen, J.; Yang, C.; Ma, L.; Ding, M. S.; Garaga, M.; Greenbaum, S.; Lee, H.-S.; Borodin, O.; Xu, K.; Wang, C. A 63 *m* Superconcentrated Aqueous Electrolyte for High-Energy Li-Ion Batteries. *ACS Energy Lett.* **2020**, *5* (3), 968–974.

(14) Han, J.; Zarrabeitia, M.; Mariani, A.; Kuenzel, M.; Mullaliu, A.; Varzi, A.; Passerini, S. Concentrated Electrolytes Enabling Stable Aqueous Ammonium-Ion Batteries. *Adv. Mater.* **2022**, *34* (32), 2201877.

(15) Liu, S.; Klukas, R.; Porada, T.; Furda, K.; Fernández, A. M.; Balducci, A. Potassium Formate-Based Electrolytes for High Performance Aqueous Electrochemical Capacitors. *J. Power Sources* **2022**, *541*, 231657.

(16) Chen, F.; Wang, X.; Armand, M.; Forsyth, M. Cationic Polymer-in-Salt Electrolytes for Fast Metal Ion Conduction and Solid-State Battery Applications. *Nat. Mater.* **2022**, *21* (10), 1175–1182.

(17) Han, J.; Mariani, A.; Zarrabeitia, M.; Jusys, Z.; Behm, R. J.; Varzi, A.; Passerini, S. Zinc-Ion Hybrid Supercapacitors Employing Acetate-Based Water-in-Salt Electrolytes. *Small* **2022**, *18* (31), 2201563.

(18) Burton, T. F.; Zhu, Y.; Droguet, L.; Jommongkol, R.; Zigah, D.; Grimaud, A.; Tarascon, J.-M.; Fontaine, O. Self-Crosslinking Poly(Ethylene Glycol) Diglycidyl Ether in Water-in-Salt Electrolytes for Minimal Hydrogen Evolution Reactions and Extended LiTFSI Solubility. *J. Electrochem. Soc.* **2022**, *169* (7), 070533.

(19) Yang, C.; Chen, J.; Ji, X.; Pollard, T. P.; Lü, X.; Sun, C.-J.; Hou, S.; Liu, Q.; Liu, C.; Qing, T.; Wang, Y.; Borodin, O.; Ren, Y.; Xu, K.; Wang, C. Aqueous Li-Ion Battery Enabled by Halogen Conversion–Intercalation Chemistry in Graphite. *Nature* **2019**, *569* (7755), 245–250.

(20) Xie, J.; Liang, Z.; Lu, Y.-C. Molecular Crowding Electrolytes for High-Voltage Aqueous Batteries. *Nat. Mater.* **2020**, *19*, 1006-1011.

(21) Kühnel, R.-S.; Reber, D.; Battaglia, C. Perspective—Electrochemical Stability of Water-in-Salt Electrolytes. *J. Electrochem. Soc.* **2020**, *167* (7), 070544.

(22) Maffre, M.; Bouchal, R.; Freunberger, S. A.; Lindahl, N.; Johansson, P.; Favier, F.; Fontaine, O.; Bélanger, D. Investigation of Electrochemical and Chemical Processes Occurring at Positive Potentials in "Water-in-Salt" Electrolytes. *J. Electrochem. Soc.* **2021**, *168* (5), 050550.

(23) Suo, L.; Oh, D.; Lin, Y.; Zhuo, Z.; Borodin, O.; Gao, T.; Wang, F.; Kushima, A.; Wang, Z.; Kim, H.-C.; Qi, Y.; Yang, W.; Pan, F.; Li, J.; Xu, K.; Wang, C. How Solid-Electrolyte Interphase Forms in Aqueous Electrolytes. *J. Am. Chem. Soc.* **2017**, *139* (51), 18670–18680.

(24) Li, C.-Y.; Chen, M.; Liu, S.; Lu, X.; Meng, J.; Yan, J.; Abruña, H. D.; Feng, G.; Lian, T. Unconventional Interfacial Water Structure of Highly Concentrated Aqueous Electrolytes at Negative Electrode Polarizations. *Nat. Commun.* **2022**, *13* (1), 5330.

(25) Zhang, H.; Gao, J.; Raciti, D.; Hall, A. S. Promoting Cu-Catalysed CO_2 Electroreduction to Multicarbon Products by Tuning the Activity of H_2O. *Nat. Catal.* **2023**, *6* (9), 807–817.

(26) Dong, Q.; Zhang, X.; He, D.; Lang, C.; Wang, D. Role of H_2O in CO_2 Electrochemical Reduction as Studied in a Water-in-Salt System. *ACS Cent. Sci.* **2019**, *5* (8), 1461–1467.

(27) Nian, Q.; Zhang, X.; Feng, Y.; Liu, S.; Sun, T.; Zheng, S.; Ren, X.; Tao, Z.; Zhang, D.; Chen, J. Designing Electrolyte Structure to Suppress Hydrogen Evolution Reaction in Aqueous Batteries. *ACS Energy Lett.* **2021**, 2174–2180.

(28) Droguet, L.; Hobold, G. M.; Lagadec, M. F.; Guo, R.; Lethien, C.; Hallot, M.; Fontaine, O.; Tarascon, J.-M.; Gallant, B. M.; Grimaud, A. Can an Inorganic Coating Serve as Stable SEI for Aqueous Superconcentrated Electrolytes? *ACS Energy Lett.* **2021**, *6* (7), 2575–2583.

(29) Dubouis, N.; Lemaire, P.; Mirvaux, B.; Salager, E.; Deschamps, M.; Grimaud, A. The Role of the Hydrogen Evolution Reaction in the Solid–Electrolyte Interphase Formation Mechanism for "Water-in-Salt" Electrolytes. *Energy Environ. Sci.* **2018**, *11* (12), 3491–3499.

(30) Bouchal, R.; Li, Z.; Bongu, C.; Le Vot, S.; Berthelot, R.; Rotenberg, B.; Favier, F.; Freunberger, S. A.; Salanne, M.; Fontaine, O. Competitive Salt Precipitation/Dissolution During Free-Water Reduction in Water-in-Salt Electrolyte. *Angew. Chem.* **2020**, 16047-16051.

(31) Feltham, A. M.; Spiro, M. Platinized Platinum Electrodes. *Chem. Rev.* **1971**, *71* (2), 177–193.

(32) Bard, A. J.; Faulkner, L. R.; White, H.S. Electrochemical Methods: Fundamentals and Applications, 3rd ed. *Wiley*, **2001**, 414-438.

(33) Degoulange, D.; Dubouis, N.; Grimaud, A. Toward the Understanding of Water-in-Salt Electrolytes: Individual Ion Activities and Liquid Junction Potentials in Highly Concentrated Aqueous Solutions. *J. Chem. Phys.* **2021**, *155* (6), 064701.

(34) Vatamanu, J.; Borodin, O. Ramifications of Water-in-Salt Interfacial Structure at Charged Electrodes for Electrolyte Electrochemical Stability. *J. Phys. Chem. Lett.* **2017**, *8* (18), 4362–4367.

(35) Williams, K.; Limaye, A.; Weiss, T.; Chung, M.; Manthiram, K. Accounting for Species' Thermodynamic Activities Changes Mechanistic Interpretations of Electrochemical Kinetic Data. *ChemRxiv.* **2022**, doi:10.26434/chemrxiv-2022-vk5z9

(36) Sheng, W.; Zhuang, Z.; Gao, M.; Zheng, J.; Chen, J. G.; Yan, Y. Correlating Hydrogen Oxidation and Evolution Activity on Platinum at Different pH with Measured Hydrogen Binding Energy. *Nat. Commun.* **2015**, *6* (1), 5848.

(37) Strmcnik, D.; Uchimura, M.; Wang, C.; Subbaraman, R.; Danilovic, N.; van der Vliet, D.; Paulikas, A. P.; Stamenkovic, V. R.; Markovic, N. M. Improving the Hydrogen Oxidation Reaction Rate by Promotion of Hydroxyl Adsorption. *Nat. Chem* **2013**, *5* (4), 300–306.

(38) Curtis, J. E.; Sinclair, T. J. Effect of Electrolyte Impurity on the Electrochemical Performance of the Lead/Tetrafluoroboric Acid/Lead Dioxide Cell. *J. Power Sources* **1978**, *3* (3), 267–276.

(39) Hatano, Y.; Watanabe, K.; Livshits, A.; Busnyuk, A.; Alimov, V.; Nakamura, Y.; Hashizume, K. Effects of Bulk Impurity Concentration on the Reactivity of Metal Surface: Sticking of Hydrogen Molecules and Atoms to Polycrystalline Nb Containing Oxygen. *J. Chem. Phys.* **2007**, *127* (20), 204707.

(40) Faenza, N. V.; Bruce, L.; Lebens-Higgins, Z. W.; Plitz, I.; Pereira, N.; Piper, L. F. J.; Amatucci, G. G. Growth of Ambient Induced Surface Impurity Species on Layered Positive Electrode Materials and Impact on Electrochemical Performance. *J. Electrochem. Soc.* **2017**, *164* (14), A3727–A3741.

(41) Koh, A.; Lee, J.; Song, J.; Shin, W. Simple and Ultrasensitive Chemically Amplified Electrochemical Detection of Ferrocenemethanol on 4-Nitrophenyl Grafted Glassy Carbon Electrode. *J. Electrochem. Sci. Technol* **2016**, *7* (4), 286–292.

(42) Sheng, W.; Gasteiger, H. A.; Shao-Horn, Y. Hydrogen Oxidation and Evolution Reaction Kinetics on Platinum: Acid vs Alkaline Electrolytes. *J. Electrochem. Soc.* **2010**, *157* (11), B1529.

(43) Durst, J.; Simon, C.; Siebel, A.; Rheinländer, P. J.; Schuler, T.; Hanzlik, M.; Herranz, J.; Hasché, F.; Gasteiger, H. A. Hydrogen Oxidation and Evolution Reaction (HOR/HER) on Pt Electrodes in Acid vs. Alkaline Electrolytes: Mechanism, Activity and Particle Size Effects. *ECS Trans.* **2014**, *64* (3), 1069–1080.

(44) Da Cunha, M. C. P. M.; De Souza, J. P. I.; Nart, F. C. Reaction Pathways for Reduction of Nitrate Ions on Platinum, Rhodium, and Platinum−Rhodium Alloy Electrodes. *Langmuir* **2000**, *16* (2), 771–777.

(45) Rebollar, L.; Intikhab, S.; Zhang, S.; Deng, H.; Zeng, Z.; Snyder, J. D.; Tang, M. H. On the Relationship between Potential of Zero Charge and Solvent Dynamics in the Reversible Hydrogen Electrode. *J. Catal.* **2021**, *398*, 161–170.

(46) Shafiee, S. A.; Aarons, J.; Hamzah, H. H. Review—Electroreduction of Peroxodisulfate: A Review of a Complicated Reaction. *J. Electrochem. Soc.* **2018**, *165* (13), H785–H798.

(47) Martínez-Hincapié, R.; Climent, V.; Feliu, J. M. Investigation of the Interfacial Properties of Platinum Stepped Surfaces Using Peroxodisulfate Reduction as a Local Probe. *Electrochim. Acta* **2019**, *307*, 553–563.

(48) Ojha, K.; Arulmozhi, N.; Aranzales, D.; Koper, M. T. M. Double Layer at the Pt(111)–Aqueous Electrolyte Interface: Potential of Zero Charge and Anomalous Gouy–Chapman Screening. *Angew. Chem., Int. Ed.* **2020**, *132* (2), 721–725.

(49) Quaino, P.; Juarez, F.; Santos, E.; Schmickler, W. Volcano Plots in Hydrogen Electrocatalysis – Uses and Abuses. *Beilstein J. Nanotechnol.* **2014**, *5*, 846–854.

(50) Seh, Z. W.; Kibsgaard, J.; Dickens, C. F.; Chorkendorff, I.; Nørskov, J. K.; Jaramillo, T. F. Combining Theory and Experiment in Electrocatalysis: Insights into Materials Design. *Science* **2017**, *355* (6321), eaad4998.

(51) Stevens, M. B.; Enman, L. J.; Batchellor, A. S.; Cosby, M. R.; Vise, A. E.; Trang, C. D. M.; Boettcher, S. W. Measurement Techniques for the Study of Thin Film Heterogeneous Water Oxidation Electrocatalysts. *Chem. Mater.* **2017**, *29* (1), 120–140.

(52) Buttry, D. A.; Ward, M. D. Measurement of Interfacial Processes at Electrode Surfaces with the Electrochemical Quartz Crystal Microbalance. *Chem. Rev.* **1992**, *92* (6), 1355–1379.

(53) Dong, S.; Wang, Y.; Chen, C.; Shen, L.; Zhang, X. Niobium Tungsten Oxide in a Green Water-in-Salt Electrolyte Enables Ultra-Stable Aqueous Lithium-Ion Capacitors. *Nano-Micro Lett.* **2020**, *12* (1), 168.

(54) Pathak, R.; Gurung, A.; Elbohy, H.; Chen, K.; Reza, K. M.; Bahrami, B.; Mabrouk, S.; Ghimire, R.; Hummel, M.; Gu, Z.; Wang, X.; Wu, Y.; Zhou, Y.; Qiao, Q. Self-Recovery in Li-Metal Hybrid Lithium-Ion Batteries via WO_3 Reduction. *Nanoscale* **2018**, *10* (34), 15956–15966.

(55) Strmcnik, D.; Castelli, I. E.; Connell, J. G.; Haering, D.; Zorko, M.; Martins, P.; Lopes, P. P.; Genorio, B.; Østergaard, T.; Gasteiger, H. A.; Maglia, F.; Antonopoulos, B. K.; Stamenkovic, V. R.; Rossmeisl, J.; Markovic, N. M. Electrocatalytic Transformation of HF Impurity to H_2 and LiF in Lithium-ion Batteries. *Nat. Catal* **2018**, *1* (4), 255–262.

(56) Droguet, L.; Grimaud, A.; Fontaine, O.; Tarascon, J. Water-in-Salt Electrolyte (WiSE) for Aqueous Batteries: A Long Way to Practicality. *Adv. Energy Mater.* **2020**, *10* (43), 2002440.

(57) Goyal, A.; Marcandalli, G.; Mints, V. A.; Koper, M. T. M. Competition between CO_2 Reduction and Hydrogen Evolution on a Gold Electrode under Well-Defined Mass Transport Conditions. *J. Am. Chem. Soc.* **2020**, *142* (9), 4154–4161.

(58) Zhang, Y.-J.; Sethuraman, V.; Michalsky, R.; Peterson, A. A. Competition between CO_2 Reduction and H_2 Evolution on Transition-Metal Electrocatalysts. *ACS Catal.* **2014**, *4* (10), 3742–3748.

(59) Ren, Y.; Yu, C.; Tan, X.; Huang, H.; Wei, Q.; Qiu, J. Strategies to Suppress Hydrogen Evolution for Highly Selective Electrocatalytic Nitrogen Reduction: Challenges and Perspectives. *Energy Environ. Sci.* **2021**, *14* (3), 1176–1193.

(60) Lazouski, N.; Schiffer, Z. J.; Williams, K.; Manthiram, K. Understanding Continuous Lithium-Mediated Electrochemical Nitrogen Reduction. *Joule* **2019**, *3* (4), 1127–1139.

(61) Lazouski, N.; Chung, M.; Williams, K.; Gala, M. L.; Manthiram, K. Non-Aqueous Gas Diffusion Electrodes for Rapid Ammonia Synthesis from Nitrogen and Water-Splitting-Derived Hydrogen. *Nat. Catal* **2020**, *3* (5), 463–469.

(62) Shen, P.; Li, X.; Luo, Y.; Guo, Y.; Zhao, X.; Chu, K. High-Efficiency N_2 Electroreduction Enabled by Se-Vacancy-Rich WSe_{2-x} in Water-in-Salt Electrolytes. *ACS Nano* **2022**, *16* (5), 7915–7925.

(63) Yang, X.-H.; Papasizza, M.; Cuesta, A.; Cheng, J. Water-In-Salt Environment Reduces the Overpotential for Reduction of CO_2 to CO_2^- in Ionic Liquid/Water Mixtures. *ACS Catal.* **2022**, *12* (11), 6770–6780.

TOC Graphic

